The Astrophysical Journal, 680:L97–L100, 2008 June 20

A LYMAN BREAK GALAXY CANDIDATE AT $z \sim 9$[1]

Alaina L. Henry,[2] Matthew A. Malkan,[2] James W. Colbert,[3] Brian Siana,[3]
Harry I. Teplitz,[3] and Patrick McCarthy[4]

Received 2008 February 6; accepted 2008 May 8; published 2008 May 28

ABSTRACT

We report the discovery of a $z \sim 9$ Lyman break galaxy candidate, selected from the NICMOS Parallel Imaging Survey as a *J*-dropout with $J_{110} - H_{160} = 1.7$. *Spitzer*/IRAC photometry reveals that the galaxy has a blue $H_{160} - 3.6$ μm color and a spectral break between 3.6 and 4.5 μm. We interpret this break as the Balmer break and derive a best-fit photometric redshift of $z \sim 9$. We use Monte Carlo simulations to test the significance of this photometric redshift, and we show that there is a 96% probability of $z \geq 7$. We estimate that the lower limit to the comoving number density of such galaxies at $z \sim 9$ is $\phi > 3.8 \times 10^{-6}$ Mpc^{-3}. If the high redshift of this galaxy is confirmed, this will indicate that the luminous end of the rest-frame UV luminosity function has not evolved substantially from $z \sim 9$ to $z \sim 3$. Still, some small degeneracy remains between this $z \sim 9$ model and models at $z \sim 2$–3; deep optical imaging (reaching $I_{AB} \sim 29$) can rule out the lower z models.

Subject headings: galaxies: evolution — galaxies: formation — galaxies: high-redshift

1. INTRODUCTION

The search for the first galaxies remains one of the primary goals of extragalactic astronomy. Surveys of distant star-forming galaxies (e.g., Lyman break galaxies [LBGs]) have resulted in determinations of luminosity functions, stellar masses, and ages of objects to $z \sim 6$ (Stanway et al. 2003; Bunker et al. 2004; Yan et al. 2006; Yoshida et al. 2006; Bouwens et al. 2006; Eyles et al. 2007; Stark et al. 2007a). The space density of galaxies at $z \sim 6$ and their apparent maturity suggest that galaxy formation must have begun at $z > 7$. Although the requirement of deep near-infrared imaging makes $z \geq 7$ difficult to observe, this is a critical epoch in the history of galaxy formation. Discovery of the first galaxy-wide bursts of star formation—the first genuine protogalaxies—is essential to understanding galaxy evolution.

Pencil-beam surveys have searched for $z \geq 8$ galaxies. In the deepest available, near-infrared data—on the Hubble Deep Field–North, the Hubble Deep Field–South, the Ultra Deep Field, and the Ultra Deep Field Parallel Fields—Bouwens et al. (2005) find three possible $z \sim 10$ galaxies. In addition, observations of gravitationally lensed galaxies have also revealed a few potential $z \geq 8$ galaxies (Richard et al. 2006, 2008). However, these deep, small-area surveys find faint candidates that are difficult to follow up on, so none of the redshifts have been confirmed by measuring their spectral energy distributions (SEDs) at longer wavelengths. This crucial test has ruled out other $z \sim 10$ candidates (Bouwens et al. 2005), including the one first presented in Dickinson et al. (2000).

Our NICMOS Parallel Imaging Survey has the unique combination of sensitivity and area to find rare, luminous *J*-dropout LBGs at $8 \leq z \leq 10$. These candidates are typically $H_{160} = 23$–25 (AB), so follow-up observations can confirm or rule out extremely high redshifts. In particular, these galaxies can be observed with the Infrared Array Camera (IRAC) on the *Spitzer Space Telescope*. We present here the first results of such a survey, in which one possible $z \sim 9$ galaxy has been discovered. We use $H_0 = 70$ km s^{-1} Mpc^{-1}, $\Omega_\Lambda = 0.7$, and $\Omega_M = 0.3$, and AB magnitudes are also used throughout.

2. OBSERVATIONS AND DATA REDUCTION

We selected *J*-dropout candidates from the NICMOS Parallel Imaging Survey (135 arcmin^2; Teplitz et al. 1998; Yan et al. 2000; Colbert et al. 2005; Henry et al. 2007). In this Letter, we have adjusted the photometry by -0.16 and -0.04 mag in J_{110} and H_{160}, respectively, according to de Jong (2006). From more than 7000 detected sources, four targets were selected from the small subset (2%) with red $J_{110} - H_{160}$ (>0.9) and no J_{110} detection above 2 σ.

We observed these NICMOS-selected *J*-dropout candidates for four, five, or six orbits each with NICMOS in the J_{110} band to confirm their red $J_{110} - H_{160}$ color. The images were drizzled according to Fruchter & Hook (1997), and the resulting point-spread function (PSF) has a FWHM $\sim 0.3''$. The 5 σ sensitivity, measured in a $0.8''$ diameter aperture, is $J_{110} = 26.3$–26.5. The NICMOS colors were measured in apertures of this size.

These four galaxies were also observed with the IRAC on *Spitzer*, at 3.6, 4.5, 5.8, and 8.0 μm, respectively. The integration times were 0.9 ks pixel^{-1} at 3.6 and 5.8 μm, and 2.8 ks pixel^{-1} at 4.5 and 8.0 μm. We used the *Spitzer* Science Center mosaicking software, MOPEX, with the drizzle algorithm to combine the images from the Basic Calibrated Data set. The output pixel size is $0.6''$, and the resulting FWHM of the PSF is $1.8''$ in the 3.6 and 4.5 μm bands, $2.0''$ in the 5.8 μm band, and $2.2''$ in the 8.0 μm band. The noise was measured by placing apertures in blank parts of the images. We chose a $2.4''$ diameter aperture to avoid contamination from nearby sources. For this small aperture, the corrections are 1.8, 1.9, 2.4, and 2.7 in the four IRAC bands (derived from point sources in our fields). The resulting 3 σ sensitivities are 0.8, 0.8, 5.8, and 3.8 μJy (total).

[1] This work is based in part on observations made with the *Spitzer Space Telescope*, which is operated by the Jet Propulsion Laboratory (JPL), California Institute of Technology, under a contract with NASA. Support for this work was provided by NASA through an award issued by JPL/Caltech. This work is also based in part on observations made with the NASA/ESA *Hubble Space Telescope*, obtained from the Space Telescope Science Institute, which is operated by the Association of Universities for Research in Astronomy, Inc., under NASA contract NAS 5-26555. These observations are associated with proposals 9484, 9865, 10226, and 10899.

[2] Department of Physics and Astronomy, Box 951547, UCLA, Los Angeles, CA 90095; ahenry@astro.ucla.edu.

[3] *Spitzer* Science Center, California Institute of Technology, 220-6, Pasadena, CA 91125.

[4] Observatories of the Carnegie Institute of Washington, Santa Barbara Street, Pasadena, CA 91101.

3. RESULTS

The resulting photometry shows that three of the four sources have SEDs that are consistent with lower z interlopers. One has $J_{110} - H_{160} = 0.4$, and it is too blue to be a viable $z > 8$ candidate. Two other sources have rising SEDs into the IRAC bands, with $H_{160} - [3.6] = 2$–3. This makes them likely lower redshift interlopers, such as dusty starburst galaxies at $z \sim 2$–4 (e.g., Chen & Marzke 2004; Labbé et al. 2005; Brammer & van Dokkum 2007; Stutz et al. 2008). The most remarkable source, however, is JD 2325+1433, which has $J_{110} - H_{160} = 1.7$ and a spectrum that is flat (in f_ν) through 3.6 and 4.5 μm (much bluer than the controversial $z \sim 6.5$ J-dropout candidate reported by Mobasher et al. 2005). These are the colors that are expected for LBGs at $8 < z < 10$.

Initially, JD 2325+1433 was only detected at 4.5 μm ($f_\nu = 1.29 \pm 0.29$ μJy), even though the 3.6 and 4.5 μm images reach the same sensitivity. Since this could be evidence for a Balmer break at a redshift of $z \sim 9$, we obtained deep (10 hr) *Spitzer* Director's Discretionary Time (DDT) observations at 3.6 and 5.8 μm to verify the break. The data are reduced in the same manner as described above, and the 3 σ sensitivity is 0.23 and 2.0 μJy at 3.6 and 5.8 μm, respectively. The candidate JD 2325+1433 is detected at 3.6 μm, with $f_\nu = 0.75 \pm 0.08$ μJy, confirming the break between 3.6 and 4.5 μm. We do not detect JD 2325+1433 at 5.8 μm, which is consistent with its flat spectrum.

Postage-stamp images of JD 2325+1433 in Figure 1 show another galaxy approximately 2.5″to the east. To test whether there is significant contamination from this source, we performed a PSF subtraction to remove it. This assumes that the nearby source is unresolved in the IRAC images, which is consistent with its NICMOS size (FWHM ~ 0.5″) and the observed IRAC FWHM (~1.8″). We then remeasure JD 2325+1433, with the nearby source removed. The resulting flux density is $f_\nu = 0.82$ and 1.25 μJy at 3.6 and 4.5 μm. This is consistent with the expectation that, at most, 2%–3% of the light from a point source at the position of the nearby source would fall in the aperture that we used for JD 2325+1433—a fraction that corresponds to, at most, 0.05 μJy.

As an independent check, we used SExtractor (Bertin & Arnouts 1996) to deblend the two sources. The resulting photometry, using the same 2.4″ diameter aperture, is consistent with aperture photometry when no correction for blending is made—$f_\nu = 0.81$ and1.33 μJy at 3.6 and 4.5 μm, respectively. Therefore, we conclude that contamination is negligible, and we make no correction to the aperture photometry. We do, however, include the scatter derived from these three measurements in our IRAC error estimates, although it is only appreciable for the 3.6 μm photometry (0.04 μJy, added in quadrature with 0.08 μJy).

3.1. *Matching IRAC and NICMOS Photometry*

To facilitate comparison with IRAC, we must estimate an aperture correction to account for missed flux in the NICMOS images. Although JD 2325+1433 does not have the signal-to-noise ratio required to characterize its morphology, we can place rough constraints on its size. We use GALFIT (Peng et al. 2002) to derive sizes and axial ratios for a few different assumed light profiles. For an exponential disk model, we find $r_s = 0.2'' \pm 0.03''$ and $a/b = 0.36 \pm 0.09$, and, for a Gaussian, we find a FWHM $= 0.53'' \pm 0.06''$ and $a/b = 0.36 \pm 0.11$. We also attempted to fit a de Vaucouleurs profile, but it was unconstrained. The uncertainties on these fits define the largest and smallest galaxy sizes, and therefore the largest and smallest aperture corrections that we can expect. To account for a possible de Vaucouleurs light profile, we add 0.15 mag of missed flux to the largest exponential disk aperture correction as found by Colbert et al. (2006). We choose an aperture correction in the center of this range, and 1 σ uncertainties to span the entire range. For a 0.9″ diameter aperture, this aperture correction is 1.18 ± 0.12. We find that this aperture size minimizes the uncertainty on the total NICMOS flux density, which includes uncertainties for both the background and the aperture correction. We apply this aperture correction to J_{110} and H_{160}, since the PSF is approximately the same for both.

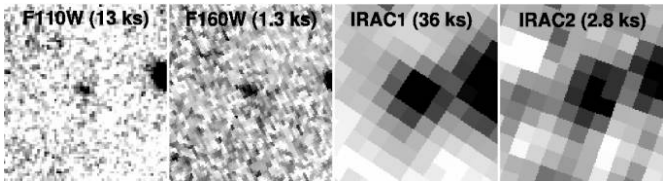

FIG. 1.—Postage-stamp images of JD 2325+1433 showing that it is elongated in the NICMOS images. Images are 6″ on a side. Note that the integration in J_{110} is 10 times longer than it is in H_{160} and that the integration in IRAC1 (3.6 μm) is 13 times longer than it is in IRAC2 (4.5 μm); so the galaxy is indeed red in $J_{110} - H_{160}$ and [3.6] − [4.5]. The coordinates of JD 2325+1433 are $23^h24^m46.52^s$, $14°32^m594^s$, bootstrapped to the 2MASS frame.

Finally, the *total* flux densities are (J_{110}, H_{160}, [3.6], [4.5]) = (0.11, 0.50, 0.75, 1.29) ± (0.03, 0.09, 0.09, 0.29) μJy. The 3 σ upper limits at 5.8 and 8.0 μm are 2.0 and 3.8 μJy, respectively.

3.2. *On the Possibility of a Stellar Contaminant*

A stellar or substellar contaminant for JD 2325+1433 is improbable, for several reasons. First, the source is likely resolved. In § 3.1, we show that the semimajor axis has a FWHM of ~0.5″, whereas the NICMOS PSF has a FWHM of ~0.35″. Furthermore, the NICMOS images in Figure 1 show that JD 2325+1433 is elongated in the same direction in both the J_{110} and H_{160} images.

Even if JD 2325+1433 were unresolved, its photometry cannot be fit by a stellar contaminant. Of particular concern are brown dwarfs, which have molecular features that can imitate spectral breaks. Although the reddest L dwarfs can fit our NICMOS color, they cannot simultaneously fit our IRAC photometry (typically $[3.6] - [4.5] \lesssim -0.5$). Similarly, T dwarfs can fit our IRAC photometry with $[3.6] - [4.5] > 0.5$ (AB), but, with $J - H < 0$, they are much too blue to fit our NICMOS observations (Burgasser et al. 2006; Patten et al. 2006). This trend in the colors of late-type T dwarfs is predicted to extend to the coolest dwarfs (Baraffe et al. 2003; T. Barman 2008, private communication). Lastly, we note that other young stellar objects such as T Tauri stars cannot produce this red $J_{110} - H_{160}$ color (e.g., Hernandez et al. 2007), as their NIR colors are dominated by photospheric emission.

4. CONSTRAINING THE REDSHIFT OF JD 2325+1433

We use the Hyperz photometric redshift code (Bolzonella et al. 2000) with Bruzual & Charlot (2003) stellar synthesis templates to estimate the redshift of JD 2325+1433. We do not include the 5.8 μm limit, as no reasonable models predict a flux $\gtrsim 2$ μJy at 5.8 μm. Assuming a Salpeter initial mass function (IMF) and using the Padova 1994 evolutionary tracks, we fit for redshift, varying age, mass normalization, extinction

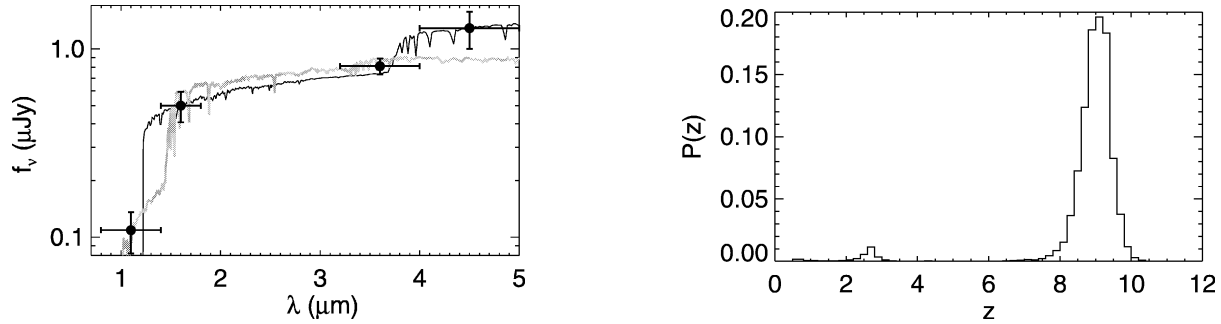

FIG. 2.—*Left*: Photometry of JD 2325+1433 showing two breaks in the spectrum, consistent with the Lyman and Balmer breaks and suggesting a redshift of $z \sim 9$. The black curve is the best-fit model ($z = 9.0$, with an age of 64 Myr, a constant SFR of 930 $M_\odot$ yr^{-1}, $A_V = 1.0$, $M_B = -23.8$, $M = 5.4 \times 10^{10}\ M_\odot$, and $Z = 0.2\ Z_\odot$). The gray curve is an alternate, poor fit at $z = 2.9$ (an instantaneous burst 360 Myr old, with $A_V = 0.1$, $M_B = -21.1$, $M = 1.8 \times 10^{10}\ M_\odot$, and $Z = Z_\odot$). *Right*: Results of our Monte Carlo simulation showing probability as a function of redshift. More than 96% of the solutions lie at $z \geq 7$.

($A_V = 0$–3; Calzetti et al. 2000 law), and metallicity ($Z = 0.005$, 0.02, 0.2, 0.4, and 1.0 $Z_\odot$). We also allow three different star formation histories: an instantaneous burst, a constant star formation rate (SFR), and an exponentially declining SFR with an *e*-folding time of 100 Myr. With four data points, the problem is underconstrained, and we are not able to estimate metallicity or star formation history. However, we include these parameters so that we do not overlook some combination of parameters that is a good fit to our data at lower redshift ($z \sim 2$–4).

In Figure 2, we compare the best-fit model (*black curve*), which has $z = 9.0$, to the best possible fit that can be achieved for $z \leq 6$ (*gray curve*). This lower z fit, which has $z = 2.9$, is significantly poorer and cannot reproduce the two breaks in the spectrum. To further test the significance of these fits, we generated 10^5 Monte Carlo realizations of the photometry, simultaneously varying the fluxes according to the measured uncertainties. We fit these data with Hyperz, as described above. The probability distribution in redshift space (see Fig. 2, *right*) shows a peak at $z = 9.0$ and a much smaller peak at $z \sim 2.5$. More than 96% of solutions lie at $z \geq 7$. This is consistent with the observed 4.5 μm flux density lying only 1.7 σ away from the $z = 2.9$ model. For normally distributed uncertainties, the true 4.5 μm flux density will lie more than 1.7 σ away from our measurement 10% of the time. This implies that there is a 5% chance that the Balmer break is more than 1.7 σ larger than we have estimated, and a 5% chance that there is no Balmer break at all. In the latter case, $z \sim 2$–3 models will be a good fit to the photometry.

In Figure 3, we show two-dimensional confidence intervals in age/redshift space and extinction/age. Estimated 1, 2, and 3 σ contours are determined from the probability at which 68.3% (95.4%, 99.7%) of the Monte Carlo realizations have a higher likelihood. In the left panel, we show that the $z \sim 9$ solution is preferred at the 1 σ level, whereas the 2 σ interval includes some $z \sim 2.5$ solutions. Both panels show that the age of JD 2325+1433 is not well constrained, with values ranging from a few Myr to several hundred Myr. The right panel shows a degeneracy between age and extinction. If we exclude models with ages less than 10 Myr (since it is unlikely that all the stars in the galaxy can form within 10 Myr), then we can also constrain the extinction to $A_V \lesssim 1$. Lastly, we note that estimated stellar masses range from 10^{10} to $10^{11}\ M_\odot$, for a Salpeter IMF.

5. IMPLICATIONS

If JD 2325+1433 is at $z \sim 9$, its UV luminosity corresponds to $5L^*(z = 3)$, and we can estimate a lower limit on the volume density of luminous $8 < z < 10$ LBGs.[5] For this redshift range, the entire NICMOS Parallel Survey covers 5.2×10^5 Mpc^3 (comoving) to $H_{160} = 24$. Beyond this, we are limited by the J_{110}-band sensitivity required to select sources with $J_{110} - H_{160} \geq 0.9$, as described in § 2. At fainter magnitudes (given the large inhomogeneity in pure parallel exposure times), 51% of the total survey area has sufficient sensitivity for us to find galaxies like JD 2325+1433. This implies that we have searched 2.6×10^5 Mpc^3 (comoving) and that the resulting volume density of $8 < z < 10$ LBGs is $\phi > 3.8 \times 10^{-6}$ Mpc^{-3}.

The volume density implied here is roughly consistent with

[5] Since we have not observed all NICMOS Parallel–selected *J*-dropout galaxies with IRAC, several more galaxies like JD 2325+1433 may exist in our survey.

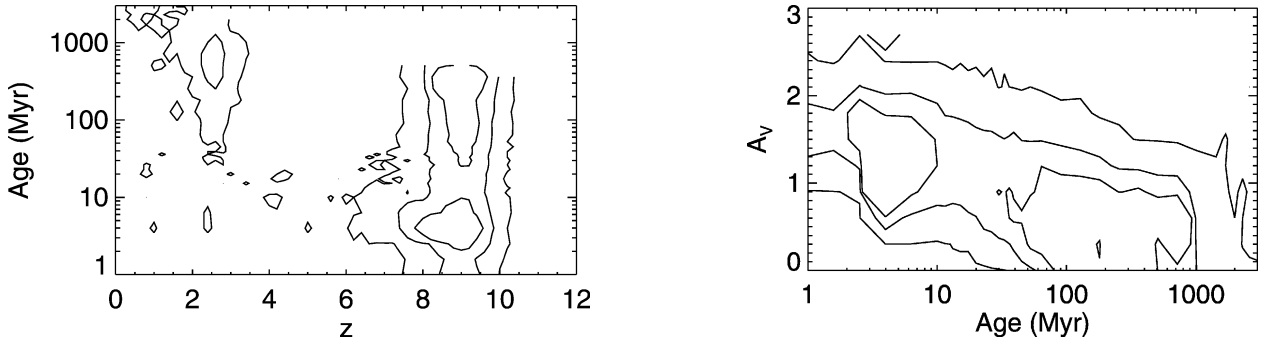

FIG. 3.—Confidence intervals show that a $z \sim 9$ solution is preferred at the 1 σ level, whereas age and extinction are not strongly constrained. Contours are 1, 2, and 3 σ. In the left hand panel, the contours are open because the best-fit ages are restricted to be younger than the age of the universe.

that at $z \sim 3$, as measured by Steidel et al. (1999). With this luminosity function (LF), we predict $\phi \sim 10^{-6}$ Mpc^{-3} for galaxies with $L > 5L^*(z = 3)$, implying 0–0.75 such sources in our survey volume (assuming Poisson errors). On the other hand, with a $z \sim 6$ LF, as measured by Bouwens et al. (2006, 2007), we predict fewer luminous galaxies and therefore a significantly smaller number for this survey (<0.001). If this $z \sim 6$ LF is representative of $z \sim 9$ LBGs, then JD 2325+1433 is almost certainly an interloper at $z \sim 2$–3. However, this evolution in the LF is uncertain, and the $z \sim 5$ LF measured by Iwata et al. (2007) shows no change in the number density of luminous galaxies from $z \sim 3$. Since the Iwata et al. survey contains 4 times more area than the Bouwens et al. survey, this measurement may be a more reliable probe of the most luminous sources.

Indirect evidence also implies that $z \geq 8$ galaxies may be detectable in the NICMOS pure parallel imaging. The ages and masses of LBGs at $z \sim 5$–6 imply a more intense period of star formation at earlier times (Yan et al. 2006; Eyles et al. 2007; Stark et al. 2007a), suggesting an upward luminosity evolution at $z > 6$. This argument is also made for faint Lyα-emitting galaxies. If any of the six candidates reported by Stark et al. (2007b) are indeed at $z > 8$, then the space density of faint Lyα emitters at this epoch must be larger than that at $z = 5.7$ (as measured by Malhotra & Rhoads 2004 and Shimasaku et al. 2006). In conclusion, the density of galaxies and the evolution of the LF at $z > 5$ are sufficiently uncertain that the $z \sim 9$ interpretation of JD 2325+1433 cannot be ruled out.

Constraining the numbers of galaxies at $z > 8$ is crucial to understanding the transition from a neutral to ionized intergalactic medium (IGM). Currently, it is unclear whether star-forming galaxies at $z \sim 6$ are capable of reionizing the IGM, largely because of the uncertainties in the stellar IMF (e.g., Chary 2008), in the escape fraction of ionizing photons (Malkan et al. 2003; Shapley et al. 2006; Siana et al. 2007), and in the gas clumping factor. If JD 2325+1433 is indeed at $z \sim 9$, the relatively large number of UV-luminous galaxies at this redshift will likely relax the requirement for strong evolution in these parameters.

Finally, we note that further observations can resolve the degeneracy between the $z \sim 9$ and $z \sim 2$–3 interpretations. The blue H_{160} − IRAC colors constrain the SED so that we can predict $I_{AB} \sim 27$–28 for the intermediate-z solutions. Of the 4% of Monte Carlo realizations (discussed in § 4) that have $z < 7$, none are fainter than $I_{AB} = 29$, so deep optical imaging can definitively confirm the redshift of JD 2325+1433.

This research was supported by NASA through *Hubble Space Telescope* Guest Observer grant 10899. We thank the *Spitzer* director, T. Soifer, for the award of the DDT. Ned Wright's Javascript Cosmology Calculator was used in preparation of this Letter. We are grateful to C. Papovich for helpful comments that improved this manuscript.

REFERENCES

Baraffe, I., Chabrier, G., Barman, T. S., Allard, F., & Hauschildt, P. H. 2003, A&A, 402, 701
Bertin, E., & Arnouts, S. 1996, A&AS, 117, 393
Bolzonella, M., Miralles, J.-M., & Pello, R. 2000, A&A, 363, 476
Bouwens, R. J., Illingworth, G. D., Blakeslee, J. P., & Franx, M. 2006, ApJ, 653, 53
Bouwens, R. J., Illingworth, G. D., Franx, M., & Ford, H. 2007, ApJ, 670, 928
Bouwens, R. J., Illingworth, G. D., Thompson, R. I., & Franx, M. 2005, ApJ, 624, L5
Brammer, G. B., & van Dokkum, P. G. 2007, ApJ, 654, L107
Bruzual, G., & Charlot, S. 2003, MNRAS, 344, 1000
Bunker, A. J., Stanway, E. R., Ellis, R. S., & McMahon, R. G. 2004, MNRAS, 355, 374
Burgasser, A. J., et al. 2006, ApJS, 166, 585
Calzetti, D., Armus, L., Bohlin, R. C., Kinney, A. L., Koornneef, J., & Storchi-Bergmann, T. 2000, ApJ, 533, 682
Chary, R.-R., 2008, ApJ, in press (astro-ph/0712.1498)
Chen, H.-W., & Marzke, R. O. 2004, ApJ, 615, 603
Colbert, J. W., Malkan, M. A., Rich, R. M., Frogel, J. A., Salim, S., & Teplitz, H. I. 2006, ApJ, 638, 603
Colbert, J. W., Teplitz, H. I., Yan, L., Malkan, M. A., & McCarthy, P. J. 2005, ApJ, 621, 587
de Jong, R. S. 2006, NICMOS Instrum. Sci. Rep. 2006-003 (Baltimore: STScI)
Dickinson, M., et al. 2000, ApJ, 531, 624
Eyles, L. P., Bunker, A. J., Ellis, R. S., Lacy, M., Stanway, E. R., Stark, D. P., & Chiu, K. 2007, MNRAS, 374, 910
Fruchter, A., & Hook, R. N. 1997, Proc. SPIE, 3164, 120
Henry, A. L., Malkan, M. A., Colbert, J. W., Siana, B., Teplitz, H. I., McCarthy, P., & Yan, L. 2007, ApJ, 656, L1
Hernandez, J., et al. 2007, ApJ, 662, 1067
Iwata, I., Ohta, K., Tamura, N., Akiyama, M., Aoki, K., Ando, M., Kiuchi, G., & Sawicki, M. 2007, MNRAS, 376, 1557
Labbé, I., et al. 2005, ApJ, 624, L81
Malhotra, S., & Rhoads, J. E. 2004, ApJ, 617, L5
Malkan, M., Webb, W., & Konopacky, Q. 2003, ApJ, 598, 878
Mobasher, B., et al. 2005, ApJ, 635, 832
Patten, B. M., et al. 2006, ApJ, 651, 502
Peng, C. Y., Ho, L. C., Impey, C. D., & Rix, H.-W. 2002, AJ, 124, 266
Richard, J., Pelló, R., Schaerer, D., Le Borgne, J.-F., & Kneib, J.-P. 2006, A&A, 456, 861
Richard, J., Stark, D. P., Ellis, R. S., George, M. R., Egami, E., Kneib, J.-P., & Smith, G. P. 2008, ApJ, submitted (astro-ph/0803.4391)
Shapley, A. E., Steidel C. C., Pettini, M., Adelberger, K. L., & Erb, D. K. 2006, ApJ, 651, 688
Shimasaku, K., et al. 2006, PASJ, 58, 313
Siana, B., et al. 2007, ApJ, 668, 62
Stanway, E. R., Bunker, A. J., & McMahon, R. G. 2003, MNRAS, 342, 439
Stark, D. P., Bunker, A. J., Ellis, R. S., Eyles, L. P., & Lacy, M. 2007a, ApJ, 659, 84
Stark, D. P., Ellis, R. S., Richard, J. S., Kneib, J.-P., Smith, G. P., & Santos, M. R. 2007b, ApJ, 663, 10
Steidel, C. C., Adelberger, K. L.,Giavalisco, M., Dickinson, M., & Pettini, M. 1999, ApJ, 519, 1
Stutz, A. M., Papovich, C., & Eisenstein, D. J. 2008, ApJ, 677, 828
Teplitz, H. I., Gardner, J. P., Malumuth, E. M., & Heap, S. R. 1998, ApJ, 507, L17
Yan, H., Dickinson, M., Giavalisco, M., Stern, D., Eisenhardt, P. R. M., & Ferguson, H. C. 2006, ApJ, 651, 24
Yan, L., McCarthy, P. J., Weymann, R. J., Malkan, M. A., Teplitz, H. I., Storrie-Lombardi, L. J., Smith, M., & Dressler, A. 2000, AJ, 120, 575
Yoshida, M., et al. 2006, ApJ, 653, 988